All-optical efficient measurement of the Verdet Constant in achiral and chiral liquid solutions: towards all-optical Magnetic-Spectroscopies

Vincent Rodriguez (vincent.rodriguez@u-bordeaux.fr)
University of Bordeaux https://orcid.org/0000-0001-6804-9757
Dominique Verreault
University of Bordeaux
Frédéric Adamietz
University of Bordeaux
Apostolos Kalafatis
University of Bordeaux https://orcid.org/0000-0002-0959-5763

Article

Keywords:

Posted Date: April 12th, 2022

DOI: https://doi.org/10.21203/rs.3.rs-1530255/v1

All-optical measurements of the Verdet constant in achiral and chiral liquids: Towards all-optical magnetic spectroscopies

Vincent Rodriguez*, Dominique Verreault, Frédéric Adamietz and Apostolos Kalafatis

Institut des Sciences Moléculaires, UMR 5255 CNRS, Université de Bordeaux, 351 Cours de la Libération, F-33405 Talence Cedex, France

Corresponding author

* vincent.rodriguez@u-bordeaux.fr

Abstract

Magneto-optical effects (MOEs) are attracting wide interest and are found in various applications including magnetic field sensors, optical modulators, isolators and switches. In this work, we have revisited the all-optical inverse Faraday effect (IFE) method to measure the Faraday rotation angle and determine the Verdet constant of diamagnetic/paramagnetic liquids and solutions. We show that by using a tunable picosecond laser source the generated IFE enables to reach magnetic flux densities in liquids in the range of 1-100 T, levels which are comparable to or higher than pulsed magnetic fields obtained using electromagnets. This all-optical method with no pump-probe scheme has the advantage that it requires small volumes (<100 µL) and enables *in situ*, fast, and efficient static measurements. We further show that it is possible to determine the Verdet constant of solutes in binary diluted solutions and demonstrate that the Verdet constants of chiral molecules exhibit significant enantiomeric difference.

Magneto-optical effects (MOEs) refer traditionally to any phenomena arising as a result of the interaction between light and an optical medium that is magnetized, whether it be spontaneously or externally by an applied quasi-static magnetic field[1,2]. MOEs usually manifest themselves through changes in the polarization state, the phase, the intensity and/or the propagation direction of light. The most well-known example of MOEs, the Faraday effect (FE)[3-7], is linear with the applied magnetic field and describes the rotation of the polarization of linearly polarized light as it travels through a non-absorbing medium in a direction parallel to an externally applied magnetic field (Faraday configuration). Phenomenologically, it can be shown that the FE arises from a second-order nonlinear optical (NLO) response of the media to the quasi-static field and that it is related to the magnetic circular birefringence (MCB), *i.e.*, the difference in the magnetized medium's refractive index for left- and right-handed circularly polarized (LCP/RCP) light (see Methods section). Because linearly polarized light can be represented as a superposition of LCP and RCP components that travels at different phase velocities c/n_L and c/n_R, its plane of polarization therefore rotates by an angle[8,9]

$$\alpha = \frac{\omega}{2c}\Delta n_{\mathrm{MCB}} L = V(\lambda) B_0 L \qquad (1)$$

where $\Delta n_{\mathrm{MCB}} = n_R - n_L$ and n_L and n_R are the refractive indices of the medium for LCP and RCP light, respectively. The handedness convention of the polarized input beam is defined here by looking towards the source, against the direction of beam propagation. B_0 is the longitudinal (*i.e.*, collinear with the light propagation direction) component of the magnetic flux density, L is the optical path length, and λ is the wavelength of the light. V is the Verdet constant, a measure of the strength of the FE, which depends on the properties of the medium, the wavelength, and the temperature. Generally, materials with positive Verdet constants are categorized as diamagnetic, whereas those with negative Verdet constant are paramagnetic[10].

A unique feature of the FE is that it is a non-reciprocal effect, meaning that the direction of rotation is independent of the direction of light propagation, unlike the natural optical rotation of chiral molecules for example which is a reciprocal effect. Hence, a beam travelling forward and backward has for effect of doubling the rotation angle. If the medium is absorbing, the refractive index becomes complex, and its real (refractive index) and imaginary (extinction coefficient) parts are different for LCP and RCP light[11]. The latter difference is referred to as magnetic circular dichroism (MCD). MCB and MCD are related to each other via Kramers-Kronig relations. In an absorbing medium, linearly polarized light not only rotates but also becomes elliptically polarized.

Clearly, the empirical law given in Eq. (1) provides a mean to find directly the Verdet constant of a material under a given magnetic field strength and for a definite optical path length by measuring the Faraday rotation angle. Using this law, the Verdet constants of various diamagnetic and paramagnetic media including gases, liquids, and solids have since been determined experimentally and at several wavelengths[12-16]. Most of these measurements relied on magnetic fields produced either by direct current (DC)[16,17], alternating current (AC)[18-20], or pulsed methods[21]. Except for the latter method, generated magnetic flux densities are relatively weak (< 1 T) and measured Faraday rotation angles are small (< 1°). To improve the detection sensitivity, modulation[22,23] and balanced photodetection[24,25] with lock-in amplifying techniques are usually supplemented. However, this has for drawback to make experimental setups bulky and expensive as they involve rare-earth-based electromagnets and complex electronics.

An alternative, albeit lesser known, approach to the generation of quasi-static magnetic field is based on so-called inverse MOEs (IMOEs) or, more properly, opto-magnetic effects. The first observation of such effects was reported in the early 60s by Pershan *et al.* when a static magnetization was optically-induced in non-absorbing materials along the propagation direction of intense circularly polarized light coming from a pulsed laser source[26]. Because the

static magnetization breaks the directional symmetry of the medium's susceptibility and leads to a circular birefringence similar to the FE, the effect was called inverse Faraday effect (IFE). Phenomenologically, it can be shown that the optically-induced magnetization results from the NLO response of the media to the optical frequency field. In fact, this effect could be view as an optomagnetic rectification since it is the magnetic analog of the optical rectification (see Methods section). The optically-induced static magnetization is based on a differential measurement of circular intensities and is given by[8,27]

$$M_0 = \frac{n_0 \lambda}{\pi c} V(\lambda)(I_R - I_L) \quad , \tag{2}$$

where I_L and I_R are the intensities of the LCP and RCP light, respectively, and n_0 the refractive index of the medium in the absence of magnetization. The presence of the Verdet constant in both Eqs. (1) and (2) immediately suggests that the coupling between the IFE and the FE could be used to determine the Verdet constant of any non-absorbing material (Fig. 1). In this scheme, a single elliptically polarized input beam induces a static magnetization in the medium with the IFE. In turn, the magnetized medium modifies the polarization characteristics of the beam through the FE and the Faraday rotation angle can be used to retrieve the Verdet constant. In their study, Pershan *et al.* demonstrated the capacity of this all-optical method by measuring the Verdet constants of a series of organic and inorganic liquids, as well as that of a paramagnetic Eu^{2+}-doped CaF_2 glass[26]. Despite the potential and simplicity (*e.g.*, no need for a pump-probe configuration) of the method, there has been to the authors' knowledge no further development nor study that were applied to the determination of Verdet constants. One plausible reason for this state-of-affairs was the high average power necessary to generate the IFE with the available pulsed nanosecond laser sources. The long pulse width (> 1 m), characteristic of these sources, has also for adverse effect to generate strong peak power on the

sample interface/holder and other optics, thus likely damaging these interfaces and limit the potential/sensibility of the method. However, we will show below that these experimental difficulties can be mitigated and that all-optical IFE/FE measurements in the nanosecond regime are possible, even at longer wavelengths (1550 nm). Another, yet unexplored, approach that would avoid such drawbacks and better match the time scale of spin-orbit interactions relevant to the IFE[28,29] would be to work instead in the picosecond regime.

Here, we revisit Pershan's IFE-based method to measure the Faraday rotation angle and determine the Verdet constants of any liquid and solution composed of diamagnetic or paramagnetic, achiral or chiral molecules. We show that picosecond laser sources are actually very efficient to generate IFE and to perform static measurements of the Verdet constant. Therefore, using a pulsed (1 kHz) picosecond laser source, tunable in the visible to near-infrared range (700-2000 nm), we were able to reach pulsed static magnetic flux densities in liquids in the range of 1-100 T, levels which are comparable to or higher than those obtained with pulsed magnetic fields. However, when time-averaged, these magnetic flux densities fall in the range of a few μT, *i.e.,* less than the Earth's average magnetic field (~40 μT), thus presenting no health risk nor potential for mechanical damages. The picosecond pulse width also physically limits the magnetic field over a smaller spatial range (< 5-7 mm), therefore reducing the sample volume down to 50-100 μL, and potentially even less. In addition, contrary to previous magnetization detection methods that imposed to do differential measurements, our approach offers the possibility to perform *in situ*, fast static measurements that can be averaged over a few seconds, thereby ensuring a high signal-to-noise ratio. By using an internal reference method, it was possible to extract the Verdet constant of an Eu(III)-triflate complex in binary dilute solutions (< 1 mM). Also, we were able to make the first demonstration of an efficient chiral discrimination by measuring the Verdet constants of enantiomers of α-pinene and carvone.

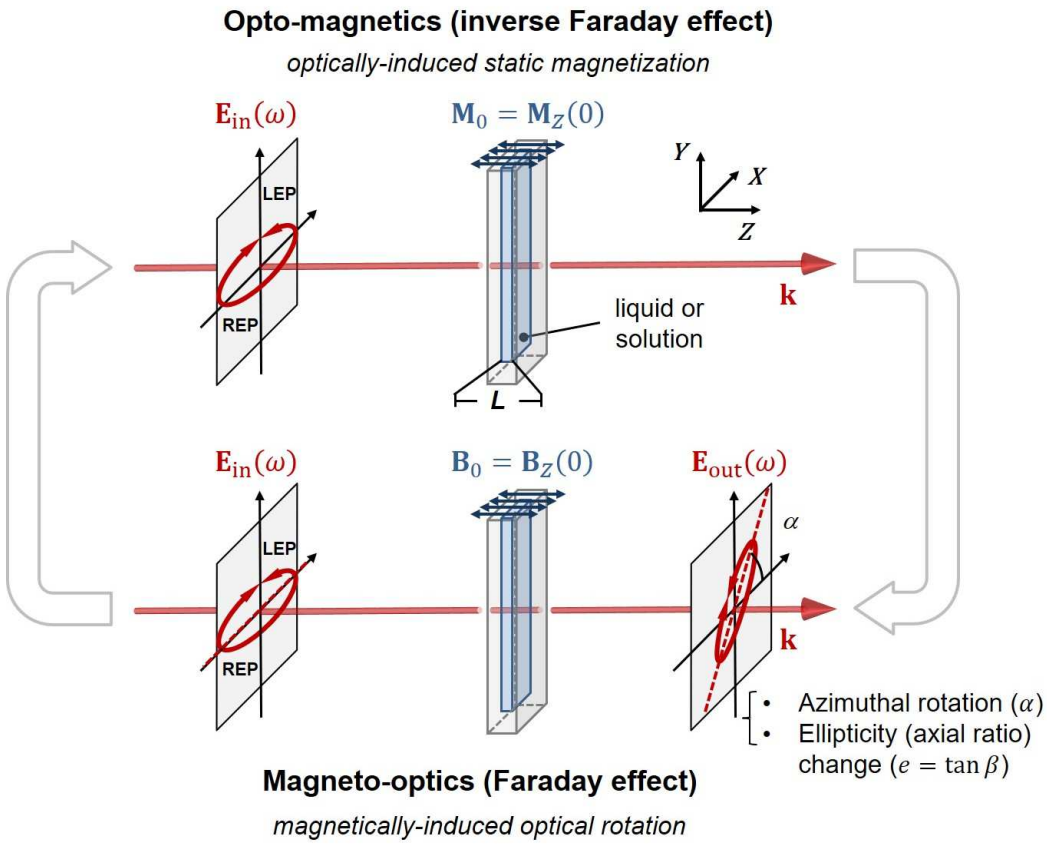

Fig. 1 Schematic illustration of the coupling between the Faraday effect (FE) and the inverse Faraday effect (IFE) in a liquid. In the IFE, the propagation of an intense left- or right-handed elliptically polarized (LEP/REP) input laser beam of frequency ω through a liquid of thickness L induces a static magnetization $\mathbf{M}_0$ collinear with the direction of propagation $\mathbf{k}$. This magnetization is equivalent to a static magnetic flux density $\mathbf{B}_0$ that acts on the LEP/REP input beam and, through the FE, changes the polarization characteristics (azimuthal rotation and ellipticity) of the output beam. The handedness convention of the polarized input beam is defined by looking towards the source, against the direction of propagation.

Results

Evidence of strong optically-induced magnetization in diamagnetic liquids. Fig. 2 illustrates the effect of the laser power of a 700 nm input beam on the azimuth (rotation angle) and ellipticity (*i.e.*, the ratio of the length of the semi-minor axis to that of the semi-major axis) of the elliptically polarized output beam after its propagation in liquid benzene over an optical path length of 2 mm (see "Determination of the characteristic parameters of the elliptical polarization" in Supporting Information for details). Benzene was chosen mainly because, unlike other organic solvents such as toluene and carbon disulfide, it offers a good compromise between a large Verdet constant[13,30] and a relatively small optical Kerr constant[31]. The effect was measured for both left- and right-handed elliptically polarized (LEP/REP) input beams. Here, the convention taken for the handedness is defined by looking towards the source, against the direction of beam propagation. As mentioned previously, through the IFE, the propagation of an elliptically polarized input beam in the liquid induces a static magnetization, which is function of the input peak power or, equivalently, the average power. In turn, this magnetization will give rise to the rotation of the major axis of the elliptical polarization due to the FE. Hence, there exists a linear relationship between the Faraday rotation angle and the input beam power in the low power regime. As seen in Fig. 2a, a strong linearity is observed up to about 1 mW for both input polarizations, after which small deviations start to appear. The onset of these deviations occurs even earlier when one looks at the ellipticity (Fig. 2b). Here, the elliptical shape of the output beam remains unchanged up to ~0.75 mW. However, at higher powers, the polarization state has a tendency to become increasingly circularly polarized.

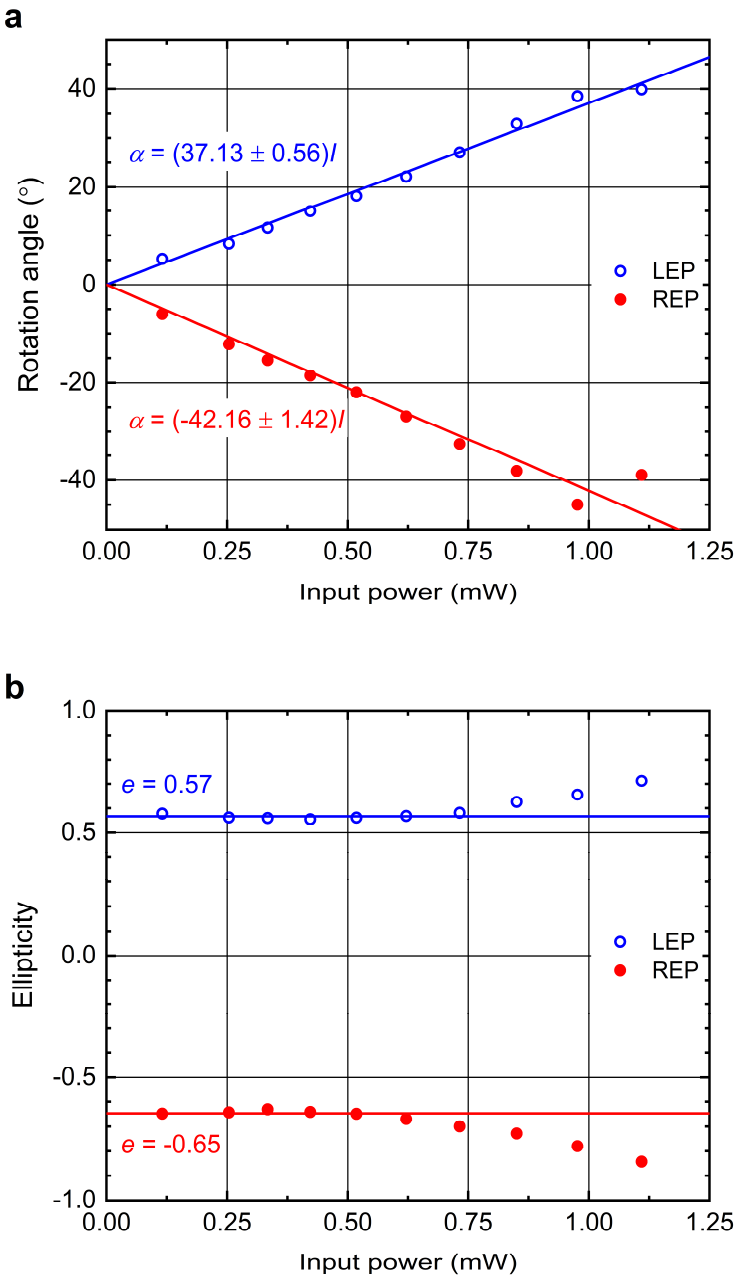

Fig. 2 Effect of the laser input power on the characteristic parameters of the elliptically polarized output beam in benzene at 700 nm. a Rotation angle. **b** Ellipticity (axial ratio). The optical path length was 2 mm. Data was taken for LEP and REP input beams. Symbols and solid lines represent data and fit, respectively.

Using the data of the rotation angle from Fig. 2 (LEP state) and the value of the Verdet constant for benzene at 700 nm (265.4° T^{-1} m^{-1})[30] fitted from the available literature datasets

(Supplementary Fig. 2a), Eq. (1) enables to calculate the magnitude of the static magnetic flux density present in the liquid. Fig. 3 shows that even under moderate average laser input powers, the static magnetic flux density in benzene reaches magnitudes in the range of 1–75 T. For example, with a 0.5 mW input beam in the LEP state, the measured rotation angle is ~18.6°, which according to Eq. (1) results in a peak magnetic flux density of ~35 T. As a consistency check, the static magnetic flux density is compared with the peak magnetic flux density of the laser input beam. With a beam waist diameter at the Rayleigh range of $2w_R \approx 10.6$ µm (Supplementary Table 1), the peak irradiance per mW is $I_{0p} \approx 57.0\ \mathrm{GW \cdot cm^{-2}}$, and the average magnetic flux density per mW $B_{\mathrm{avg}} = 2.29 \times 10^{-7}\ V = 1.1$ µT. With a laser with a repetition rate of $f_{\mathrm{rep}} = 1$ kHz and pulse duration of $\tau = 22.5$ ps, the peak magnetic flux density at 0.5 mW is therefore given by $B_{\mathrm{pk}} = B_{\mathrm{avg}}/\tau f_{\mathrm{rep}} \approx 47$ T, a value that falls in the range found above. The discrepancy with the value deduced from the rotation angle likely comes from the estimation of the beam irradiance which strongly depends on the location where the beam waist diameter is taken.

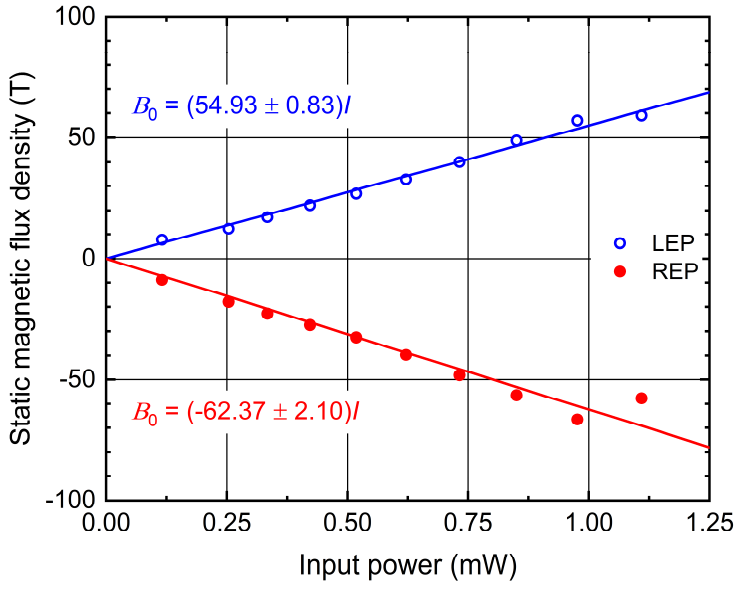

Fig. 3 Optically-induced static magnetic flux density in benzene at 700 nm. The input power range is the same as in Fig. 2. The Verdet constant used for benzene at 700 nm is $V = 265.4° \cdot T^{-1} \cdot m^{-1}$ (Table 1)[30]. The optical path length was 2 mm. Data was taken for LEP and REP input beams. Symbols and solid lines represent data and fit, respectively.

To verify that the IFE and the corresponding optically-induced static magnetization are developed over the spatial extent of the laser pulse, the rotation angle was measured in chloroform for different cell lengths (Fig. 4). According to Eq. (1), it is shown that the rotation angle is very linear with the cell length (L) for the smaller cells up to 5 mm. However, for the largest cell there is a clear deviation, indicating that the cell length has exceeded the spatial extent of the optical pulse and the static magnetization it generates. For a pulse duration of $\tau \approx$ 20–25 ps duration, the spatial extent is $l = c\tau \approx$ 6–7.5 mm. Hence, beyond this limit, the IFE becomes weaker and the static magnetization cannot be fully induced. For the experimental work on liquids and solutions, the cell length (optical path) was chosen to be less than or equal to 5 mm.

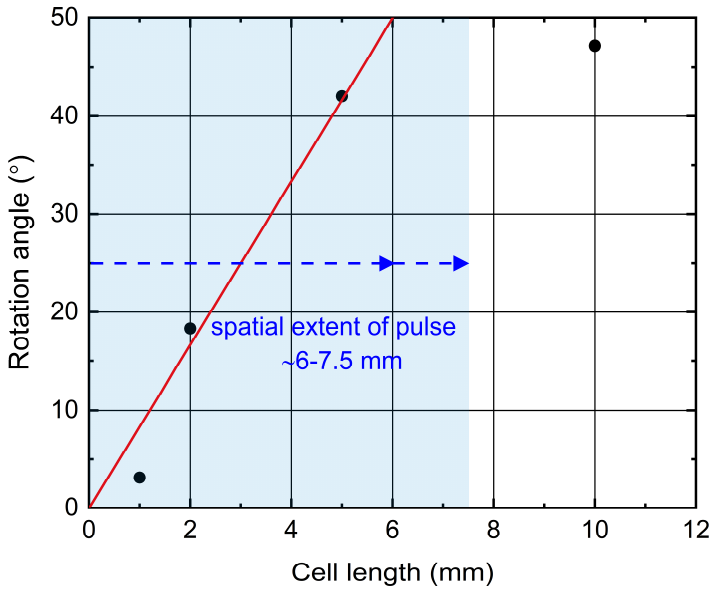

Fig. 4 Rotation angle in chloroform at 700 nm as function of cell length. The input power was set to 1.7 mW and the input polarization state was LEP. Symbol and line represent data and fit, respectively. The spatial extent of the optical pulse (blue area) is shown for comparison.

The effect of the input laser power on the rotation angle and ellipticity of the output beam was checked for different input polarization states by varying the half-wave plate (HWP) rotation angle ψ which changes implicitly the characteristic parameters (χ, φ) and the H factor of the output polarization (see Eqs. (24) and (25) in the Methods section). The dependence of the H factor on the HWP rotation angle ψ is shown in Supplementary Fig. 3. Fig. 5a shows that at low input power (0.9 mW) there is no rotation measured for the linearly polarized (LP; $\psi = 0°$) input beam indicating that, as expected, no IFE and, in turn, no magnetization optically-induced of the liquid. In addition, we do not see any linear birefringence (LB) (no change of ellipticity) due to the optical Kerr effect (OKE) as reported in Supplementary Fig. 4a. In the case of LCP/RCP ($\psi = \pm 22.5°$) input beams, the IFE is maximized but the maximum induced static magnetic flux density cannot change the input polarization state as LCP and RCP are the proper polarization states in magneto-optical media. Hence, no Faraday rotation can be probed with a circular polarization. For any other elliptical polarization states, which are not proper polarization states, a Faraday rotation occurs partially induced by the IFE/FE, depending on the relative asymmetry of the optical field in relation with the value of ψ, *i.e.*, (χ, φ) (see Eq. (25) in the Methods section). In contrast, at higher input powers (2.4 mW) (Fig. 5b), Faraday rotation occurs more efficiently but OKE induces a LB as shown by the change of ellipticity (Supplementary Fig. 4b). It occurs with linearly polarized input beams as well as with any elliptical polarization states. Even though chloroform has a fairly modest OKE constant, for instance, in comparison to benzene and its derivatives[31], the performed photopolarimetric measurement is quite sensitive to the influence of LB effects that have $\mathbf{E}^2$- or $\mathbf{H}^2$-dependencies,

including potential Cotton-Mouton effect (CME) and inverse CME (ICME)[28,29]. The effect of input laser power had also similar effects on the ellipticity, with LB effects causing the output beams to become more circular (Supplementary Fig. 4).

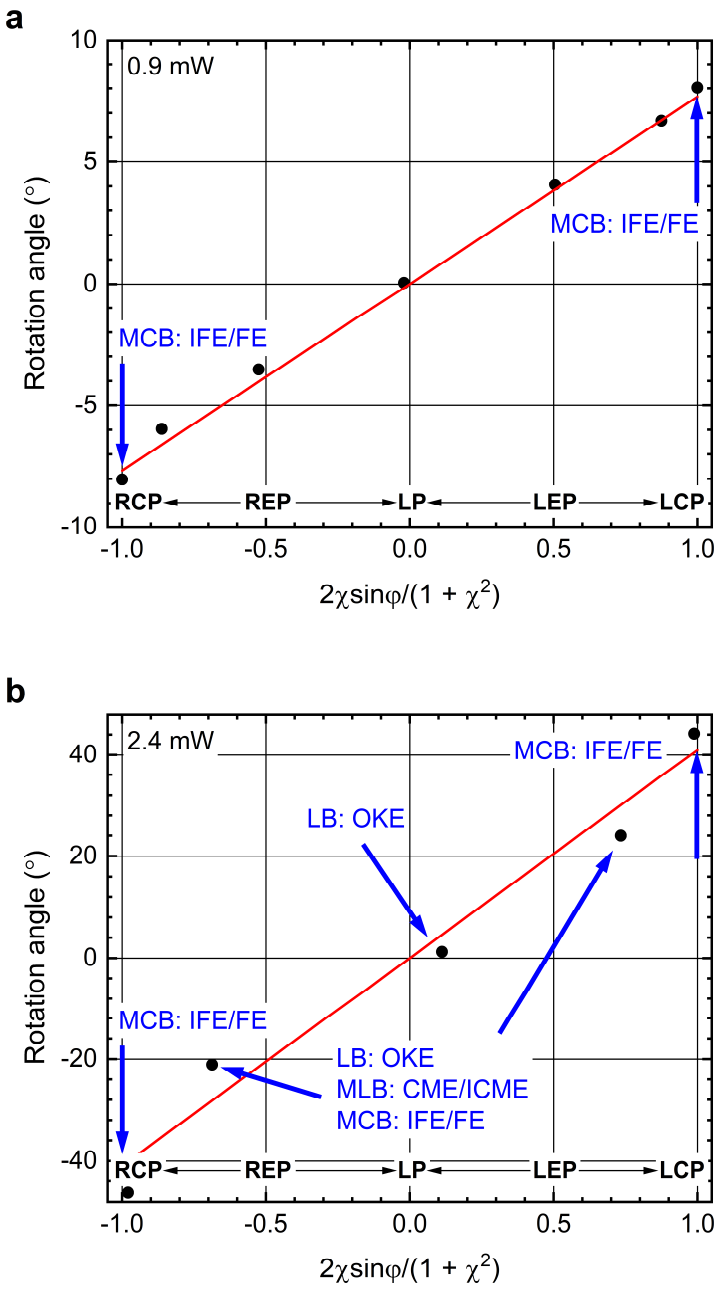

Fig. 5 Effect of the laser input power on the rotation angle in chloroform at 700 nm for different input polarization states. a Low power (0.9 mW). **b** High power (2.4 mW). The

optical path length was 2 mm. Symbol and line represent data and fit, respectively. The fit represents the rotation angle when only contributions from IFE/FE are present.

Calibration method of the Verdet constant. External reference method. The fact that the rotation angle of benzene is linear over most of the input powers investigated and that this linear regime is where FE and IFE are predominant effects, enables to use benzene as a reference solvent to determine the Verdet constants of other diamagnetic liquids, provided they also display some linearity over the same (or lower) range of input powers. To demonstrate this external reference method, the rotation angle of chloroform was measured in the same experimental conditions as for benzene. Fig. 6 shows the rotation angle of chloroform plotted as function of the laser input power. Here, the input power range was extended because chloroform has an even weaker optical Kerr constant than benzene[31]. Recalling that the rotation angle in the linear regime is of the form $\alpha = mI$, where $m = G(\lambda, \chi, \varphi)LV^2$ is the slope (see Eq. (25) in Methods section), then from the comparison between the slopes of a reference solvent and another solvent at a given wavelength λ, the unknown Verdet constant of the latter is determined by

$$V_{\mathrm{svt}}^{\lambda} = (\alpha_{\mathrm{svt}}/\alpha_{\mathrm{ref}})^{1/2} V_{\mathrm{ref}}^{\lambda} = (m_{\mathrm{svt}}/m_{\mathrm{ref}})^{1/2} V_{\mathrm{ref}}^{\lambda} \quad , \tag{3}$$

where $V_{\mathrm{ref}}^{\lambda}$ and $V_{\mathrm{svt}}^{\lambda}$ are the Verdet constants at the wavelength λ of the reference and unknown solvent, respectively.

Considering without loss of generality only the LEP state, one finds from the linear fit of the rotation angle of benzene (Fig. 2) that $m_{\mathrm{ref}} \approx (37.13 \pm 0.56)I$, whereas for chloroform one has $m_{\mathrm{svt}} \approx (9.05 \pm 0.74)I$. Taking the fitted value of the Verdet constant of benzene at 700 nm, $V_{\mathrm{ref}}^{700} = 265.4\,^{\circ} \cdot \mathrm{T}^{-1} \cdot \mathrm{m}^{-1}$ (Supplementary Fig. 2a) from Botek *et al.*[30], the calculated

Verdet constant for chloroform at 700 nm is $V_{\mathrm{svt}}^{700} \approx 131.1 \pm 5.5\,^{\circ} \cdot \mathrm{T}^{-1} \cdot \mathrm{m}^{-1}$, in good agreement with values at 700 nm obtained from fitting of literature datasets (Table 1). It is important to note that, under strong applied or optically-induced magnetic fields, higher-order MOEs and IMOEs occurs, such as the CME and ICME, which are quadratic with the magnetic field and correspond to magnetic linear birefringence (MLB) contributions. However, the current determination of the Verdet constant is done in the low power regime where the slope at the origin depends linearly on the Verdet constant.

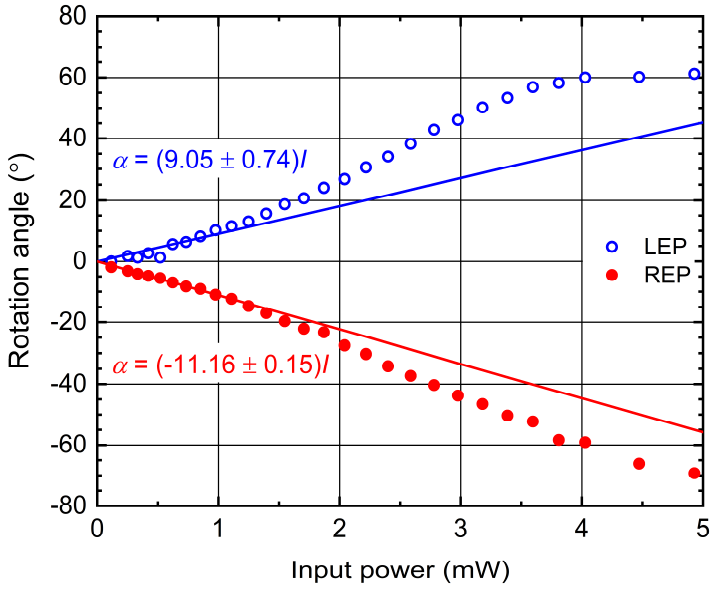

Fig. 6 Effect of the laser input power on the rotation angle of the elliptically polarized output beam in chloroform at 700 nm. The optical path length was 2 mm. Data was taken for LEP and REP input beams. Symbols and solid lines represent data and fit, respectively.

To further validate the method and for comparison purpose, it was applied to two other solvents, toluene and water. The plots of rotation angle for these solvents as function of the laser input

power in the LEP state are given in Supplementary Fig. 5. The Verdet constants of these solvents calculated with the external reference method are found in Table 1.

Table 1. Comparison between Verdet constants of diamagnetic liquids calculated with the external reference method and those obtained from fitting of available literature datasets (Supplementary Fig. 2).

solvent	V_{svt}^{700} $(^\circ \cdot \mathrm{T}^{-1} \cdot \mathrm{m}^{-1})$	V_{ref}^{700} $(^\circ \cdot \mathrm{T}^{-1} \cdot \mathrm{m}^{-1})$
benzene (ref.)	**265.4**[30]	337.2[32], 334.0[13], **265.4**[30]
chloroform	131.1 ± 5.5	189.2[32], 188.9[33]
toluene	244.7 ± 5.6	306.4[32], 301.8[13], 236.2[30]
water	74.5 ± 0.8	145.5[32], 152.2[33], 152.1[13]

Comparative measurements of the Verdet constant between picosecond and nanosecond laser sources. In the previous sections, it was shown that with a laser source with an irradiance in the tens of GW·cm^{-2} and a pulse duration of tens of ps, it is possible to optically-induced a strong static magnetic field in liquids, provided that the cell length remains within the spatial extent of the pulse. In the case of nanosecond laser sources, the irradiance is usually lower by two to three orders of magnitudes, but the spatial extent of the pulse is very long (typically > 1 m) such that the liquid and the cell are involved in the interaction. Using a laser source at 1550 nm with a 5 ns pulse duration (see Methods section) with a peak irradiance per mW of $I_{0p} \approx 6.4\ \mathrm{GW} \cdot \mathrm{cm}^{-2}$, the rotation angle of benzene was measured using a cell length of 10 mm (Supplementary Fig. 6). It was necessary to found a balance between peak power and average power by adjusting the repetition rate of the ns laser (ranging from 10 to 1000 Hz). A high peak power increases the IFE/FE but also the risk of serious optical damages to the window cell (a

direct laser writing process is generated). Hence, for this specific measurement, the repetition rate of the laser was set to 50 Hz while keeping a sufficient peak power. Even though the Verdet constant of benzene at 1550 nm is relatively weak (62.2°·T^{-1}·m^{-1}; Supplementary Fig. 2a)[32] and that static measurements are render difficult by fluctuations of the nanosecond laser pulses at low repetition rate, a substantial magnetic flux density is present in the liquid at this wavelength. For example, with a 7 mW input beam in the LEP state, the measured rotation angle is 2.2°, which according to Eq. (1) results in a peak magnetic flux density of ~3.5 T. A consistency check using the data shown in Supplementary Fig. 6 shows that the average magnetic flux density in this particular setup is ~0.9 μT, which is about three orders of magnitude stronger than that obtained by Pershan *et al.* with their nanosecond laser system[26]. Considering the parameters of the nanosecond laser source (Supplementary Table 1), then for a beam waist diameter at the Rayleigh range of $2w_R \approx 9.4$ μm, one obtains a peak irradiance per mW, $I_{0p} \approx 45.7\ \mathrm{GW \cdot cm^{-2}}$, which translates into a peak magnetic flux density $B_{\mathrm{pk}} = B_{\mathrm{avg}}/\tau f_{\mathrm{rep}} \approx 3.5$ T, in perfect agreement with the value deduced from the Faraday rotation angle measurement.

Determination of the Verdet constant of binary dilute solutions. Internal reference method. For a binary solution where solute and solvent both contribute to the Faraday effect, the rotation angle relates to the Verdet constants of the two components:

$$\begin{aligned} \alpha_{\mathrm{sln}} &= mV_{\mathrm{sln}}^2 I \\ &= m\left(V_{\mathrm{svt}} + C_{\mathrm{ste}}V_{m,\mathrm{ste}}\right)^2 I \approx mV_{\mathrm{svt}}^2\left[1 + 2C_{\mathrm{ste}}\left(V_{m,\mathrm{ste}}/V_{\mathrm{svt}}\right)\right]I, \end{aligned} \tag{4}$$

where V_{svt} is the Verdet constant of the solvent, and $V_{m,\mathrm{ste}}$, C_{ste} are, respectively, the *molar* Verdet constant and molar concentration of the solute. In the last step of Eq. (4), the quadratic

terms in the solute concentration have been neglected considering very dilute solutions (< 1 mM) as long as $C_{\mathrm{ste}}V_{m,\mathrm{ste}} \ll V_{\mathrm{svt}}$. Eq. (4) enables to determine the Verdet constant of a particular solute in a solvent provided that the Verdet constant of the solvent is known. This method is referred to as the internal reference method. To demonstrate the method, the rotation angle of a 10^{-4} M Eu(III)-triflate salt complex ($Eu(Otf)_3$ where $Otf^- = CF_3SO_3^-$) dissolved in chloroform was measured in the same experimental conditions as for neat chloroform. A plot of the rotation angles of the $Eu(Otf)_3$ solution and chloroform as function of the laser input power indicates that the binary dilute solution contains as expected a paramagnetic contribution from the rare-earth Eu^{3+} cation that decrease (here slightly) the slope of the diamagnetic chloroform.

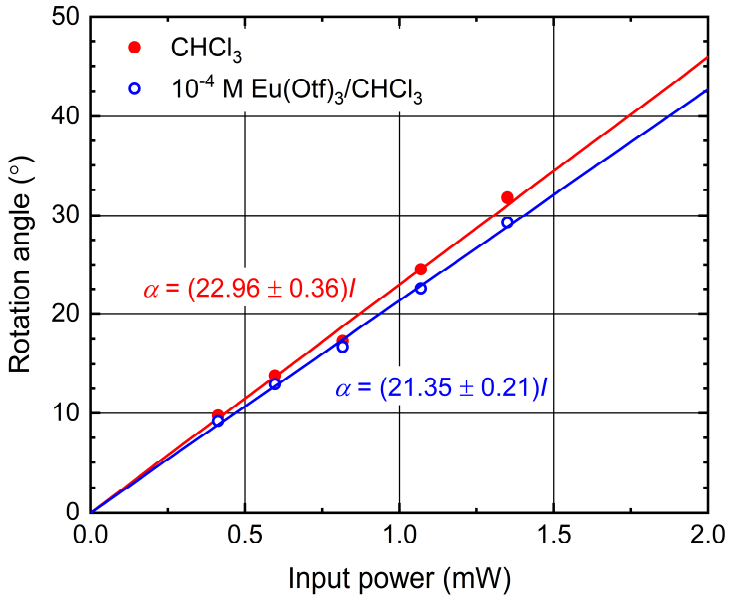

Fig. 7 Rotation angle as function of the laser input power of a 10^{-4} M $Eu(Otf)_3$ complex dissolved in chloroform at 700 nm. Rotation angle of neat chloroform is also shown for comparison. The optical path length was 5 mm. Data and fit are represented by circles and solid lines, respectively.

Comparing the slopes of the solvent (chloroform) and that of the $Eu(Otf)_3$ complex in chloroform, the unknown molar Verdet constant of the solute $Eu(Otf)_3$ is determined by

$$V_{m,\mathrm{ste}} = (V_{\mathrm{svt}}/2\,C_{\mathrm{ste}})[(\alpha_{\mathrm{sln}}/\alpha_{\mathrm{svt}}) - 1] \quad . \tag{5}$$

Considering without loss of generality only the LEP state, one finds from the linear fit of the rotation angle of chloroform that $\alpha_{\mathrm{svt}} \approx (22.96 \pm 0.36)I$ (Fig. 7), whereas for the $Eu(Otf)_3$ solution one has $\alpha_{\mathrm{sln}} \approx (21.35 \pm 0.21)I$, and taking $V_{\mathrm{svt}} = 131.1\,^{\circ} \cdot \mathrm{T}^{-1} \cdot \mathrm{m}^{-1}$ for chloroform at 700 nm (see Table 1), then the calculated Verdet constant of $Eu(Otf)_3$ at 700 nm is $V_{m,\mathrm{ste}} \approx -45965^{\circ} \cdot \mathrm{T}^{-1} \cdot \mathrm{m}^{-1} \cdot \mathrm{M}^{-1} = -77608^{\circ} \cdot \mathrm{T}^{-1} \cdot \mathrm{m}^{-1} \cdot (\mathrm{g/mL})^{-1}$.

Determination of the Verdet constant and enantiomeric difference of chiral liquids and their mixtures. Measurements of the Faraday rotation angle can also be used for the chiral discrimination between two enantiomers in a mixture. To show the potential of the method, rotation angle measurements were performed on mixtures of α-pinene enantiomers as shown in Supplementary Fig. 7. Considering a binary mixture of two enantiomers, and assuming their Verdet constants to be additive, the rotation angle of the mixture is given by

$$\begin{aligned} \alpha_{\mathrm{mix}} &= FV_{\mathrm{mix}}^2 I \\ &= F(X_S V_S + X_R V_R)^2 I = FV_S^2[(1 - X_R) + X_R(V_R/V_S)]^2 I\,, \end{aligned} \tag{6}$$

where $F = G(\lambda, \psi)L$ is a constant factor containing experimental parameters, V_i and X_i $(i = S, R)$ are the Verdet constants and volume fractions of the pure enantiomers. Fig. 8a shows the variation of the slope FV_{mix}^2 as function of the volume fraction of the enantiomers. One can clearly discriminate the two enantiomers as (1*S*)-(-)-α-pinene display a larger optical

rotation than (1*R*)-(+)-α-pinene because both natural and magnetic optical rotations are occurring in the same sense for (1*S*)-(-)-α-pinene. In contrast, for (1*R*)-(+)-α-pinene, the optical rotation is opposite to the Faraday rotation, therefore reducing its value. For example, in the case of (1*S*)-(-)-α-pinene, with a specific rotation extrapolated at 700 nm of $[\alpha]_{700} = -29° \cdot \mathrm{dm}^{-1} \cdot (\mathrm{g/mL})^{-1}$ [34], an enantiomeric excess of 97%, and a density $\rho = 0.86\ \mathrm{g/mL}$, the calculated natural optical rotation angle amounts to about -1.2° for an optical path of 5 mm. Note however that this angle of rotation is for a linear input polarization; for the LEP state with ellipticity $e = 0.6$ used here, it is estimated to be less than half of this value.

As with other achiral liquids, the Verdet constants of pure enantiomers or any of their binary mixtures can be determined using the external reference method taking this time chloroform as the reference solvent. For example, from a comparison between the slopes of chloroform and pure (1*S*)-(-)-α-pinene (Supplementary Fig. 7), the Verdet constant of (1*S*)-(-)-α-pinene at 700 nm can be determined as

$$V_S^{700} = \left(\alpha_S^{700}/\alpha_{\mathrm{ref}}^{700}\right)^{1/2} V_{\mathrm{ref}}^{700} = \left(m_S^{700}/m_{\mathrm{ref}}^{700}\right)^{1/2} V_{\mathrm{ref}}^{700} \approx 98.9\,° \cdot \mathrm{T}^{-1} \cdot \mathrm{m}^{-1}\ , \qquad (7)$$

where $V_{\mathrm{ref}}^{700} \approx 131.1\,° \cdot \mathrm{T}^{-1} \cdot \mathrm{m}^{-1}$ as determined previously (Table 1). Using the same procedure, the Verdet constant of (1*R*)-(+)-α-pinene can be determined from Eq. (7), which yields $V_R^{700} = (m_R^{700}/m_S^{700})^{1/2} V_S^{700} \approx 89.5\,° \cdot \mathrm{T}^{-1} \cdot \mathrm{m}^{-1}$. Based on these values, one can calculate the enantiomeric difference $\mathrm{ED\%} = 100 \times (|\Delta V|/\langle V \rangle) = 100 \times 2(|V_R - V_S|/V_R + V_S) \approx 10.0$ for α-pinene, thus demonstrating the sensitivity of the IFE method to perform chiral discrimination, even for small and weakly FE-active chiral molecules. Similarly, using the external reference method with chloroform as the reference, the Verdet constants of the enantiomers of carvone, another chiral standard, were determined at 775 nm with an optical path of 3 mm as shown in Supplementary Fig. 8. The Verdet constants for the

(*R*)-(-)-carvone and (*S*)-(+)-carvone were found to be 151.3 and 182.2°·T^{-1}·m^{-1}, respectively, resulting in an ED% ≈ 18.5.

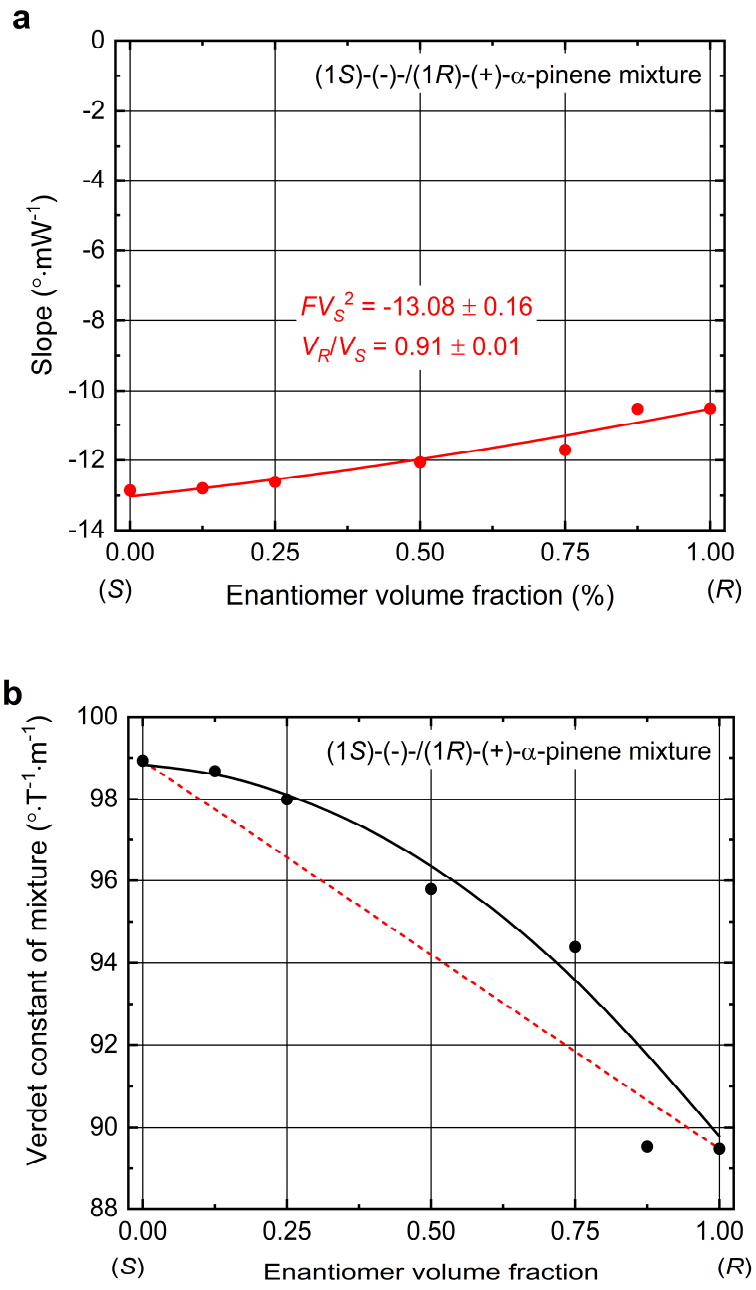

Fig. 8 Chiral discrimination of α-pinene enantiomers and Verdet constants of chiral binary mixtures. a Slope of Eq. (6) in (1*S*)-(-)/(1*R*)-(+)-α-pinene mixtures at 700 nm. The optical path length was 5 mm. Data and fit are represented by red filled circles and solid lines,

respectively. **b** Verdet constants of (1*S*)-(-)/(1*R*)-(+)-α-pinene mixtures as function of the concentration in volume fractions of the (*R*)-enantiomer at 700 nm. Ideal behavior is indicated by the red dashed line. Data and fit (eye guide) are represented by black filled circles and solid lines, respectively.

To verify whether the Verdet constant is additive in the chiral α-pinene mixture, the calculated Verdet constants were plotted as function of the volume fraction of one enantiomer (here, (1*R*)-(+)-α-pinene) (Fig. 8b). Clearly, the Verdet constant is not additive in the mixture and the deviation from ideality is positive (with the exception of one outlying concentration). Such deviation would suggest that each enantiomer has more favorable interactions with its own kind rather than with its mirror image leading to local density changes in the mixture. Similar positive deviations of the Verdet constant have also been previously observed in binary mixtures of achiral liquids[13].

Summary. For the determination of the Verdet constant of materials, current methods rely almost exclusively on externally applied magnetic fields from electromagnets. Here, we used an all-optical, single beam method that exploits the IFE to induce in liquids localized magnetic flux densities in the range of 1–100 T. We note that the IFE is more efficiently generated by using pulsed laser sources in the picosecond regime.

We find that this all-optical method requires only small sampling volumes and enables fast static measurements of the Faraday angle in any kind of liquids or solutions, whether diamagnetic or paramagnetic, achiral or chiral. We show that it is possible to extract the Verdet constant of solutes in very dilute binary solutions. In addition, we demonstrate for the first time

that the Verdet constants of chiral liquids can be used to easily discriminate enantiomers. Even for small chiral standards like α-pinene, enantiomeric differences of at least 10% are achieved.

We conclude that the all-optical, IFE-based method significantly enhances the capability in determining Verdet constant and for chiral discrimination, and opens up the possibility towards other all-optical magnetic spectroscopies.

Methods

Theory. The phenomenological theory of the FE and IFE is already well established[8,9,27,35,36], but a brief account is given here for the sake of completeness and for the convenience of the reader. In the presence of a low-frequency (quasi-static) magnetic field $\mathbf{H}_0 = \mathbf{H}(0)$, the effective susceptibility $\boldsymbol{\chi}_{\text{eff}}$ of a medium is a function of $\mathbf{H}_0$. For a sufficiently weak field (and neglecting spatial dispersion), the effective susceptibility can be expanded up to the first order in the magnetic field as

$$\boldsymbol{\chi}_{\text{eff}}(\omega, \mathbf{H}_0) = \boldsymbol{\chi}^{(1)ee}(\omega) + \mu_0\left[\boldsymbol{\chi}^{(2)eem}(\omega) + \boldsymbol{\chi}^{(2)eme}(\omega)\right] \cdot \mathbf{H}_0 \quad , \tag{8}$$

where $\boldsymbol{\chi}^{(1)ee}$ is the linear electric susceptibility arising from pure linear optical contributions, $\boldsymbol{\chi}^{(2)eem}$ and $\boldsymbol{\chi}^{(2)eme}$ are the first nonlinear susceptibility corrections that originate from mixed magneto-optical contributions, and $\mu_0 = 4\pi \times 10^{-7}$ H·m^{-1} (Fig. 9).

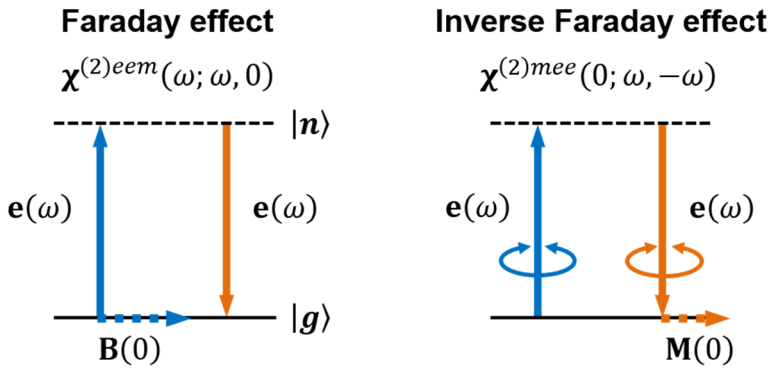

Fig. 9 Energy level diagrams of the FE and IFE. These nonlinear second-order effects are related to the mixed magneto-optical susceptibility $\boldsymbol{\chi}^{(2)eem}$ (and $\boldsymbol{\chi}^{(2)eme}$) and opto-magnetic susceptibility $\boldsymbol{\chi}^{(2)mee}$, respectively. $\mathbf{e}(\omega)$ denotes an electric dipole moment transition at frequency ω between the ground and virtual excited levels. $\mathbf{B}(0)$ and $\mathbf{M}(0)$ refer to the static magnetic flux density and static magnetization, respectively. Transitions and static field quantities are represented, respectively, by solid and dashed arrows. Note that the IFE is the magnetic analog of the optical rectification, since the static magnetization results from the difference frequency of two electric dipole transitions. Any type of input polarization states is permitted in the FE but the IFE is only possible for elliptically (including circularly) polarized light.

The effective polarization density due to this radiation source is given by

$$\mathbf{P}_{\text{eff}}(\omega,\mathbf{H}_0)=\varepsilon_0\boldsymbol{\chi}_{\text{eff}}(\omega,\mathbf{H}_0)\cdot\mathbf{E}(\omega)\quad . \tag{9}$$

Assuming a circularly polarized light travelling in the medium along the positive Z-axis with an associated time-harmonic electric field (in the frequency domain) given by

$$\mathbf{E}^{\pm}(\omega) = \frac{E_0}{\sqrt{2}}\left(\hat{\mathbf{X}} \pm i\hat{\mathbf{Y}}\right)e^{-i\omega t}\,, \tag{10}$$

where the plus (+) and minus (-) signs refer to LCP and RCP light, respectively, and a quasi-static magnetic field that is collinear with the propagation direction ($\mathbf{H}_{0Z} = H_0\hat{\mathbf{Z}}$), then the effective polarization density becomes

$$\begin{aligned}\mathbf{P}_{\text{eff}}(\omega, \mathbf{H}_0) &= \varepsilon_0\left[\boldsymbol{\chi}^{(1)ee}(\omega) \pm i\mu_0\left(\boldsymbol{\chi}^{(2)eem}(\omega) + \boldsymbol{\chi}^{(2)eme}(\omega)\right)\cdot\mathbf{H}_{0Z}\right]\cdot\mathbf{E}^{\pm}(\omega) \\ &= \varepsilon_0\boldsymbol{\chi}_{\text{eff}}^{\pm}\!:\mathbf{E}^{\pm}(\omega)\mathbf{H}_{0Z}\quad,\end{aligned} \tag{11}$$

with $i = \sqrt{-1}$. The handedness convention of the polarized input beam (Eq. (10)) is defined by looking towards the source, against the direction of beam propagation.

The refractive index of the medium (assuming that it is non-magnetic ($\mu_r = 1$)) is given by

$$\begin{aligned}n_{\pm} = \left(1 + \chi_{\text{eff}}^{\pm}\right)^{1/2} &= \left[\left(1 + \chi^{(1)ee}\right) \pm i\mu_0\left(\chi_{XYZ}^{(2)eem} + \chi_{YZX}^{(2)eme}\right)H_0\right]^{1/2} \\ &= n_0\left[1 \pm i\mu_0 n_0^{-2}\left(\chi_{XYZ}^{(2)eem} + \chi_{YZX}^{(2)eme}\right)H_0\right]^{1/2}.\end{aligned} \tag{12}$$

where n_+ and n_- are the refractive indices for LCP and RCP light, respectively, and n_0 is the refractive index of the medium in the absence of magnetic field. The frequency dependence of Eq. (12) was omitted for clarity. Because $\left(\chi_{XYZ}^{(2)eem} + \chi_{YZX}^{(2)eme}\right)H_0 \ll 1$, Eq. (12) can be expanded to yield

$$n_{\pm} \approx n_0 \pm i(\mu_0/2n_0)\left(\chi_{XYZ}^{(2)eem} + \chi_{YZX}^{(2)eme}\right)H_0\quad. \tag{13}$$

Eq. (13) as for consequence that if a LP light passes through an isotropic but optically inactive medium subject to a quasi-static magnetic field (externally applied or optically-induced), the polarization plane of the incident light will be rotated. Because the LP light can be decomposed into LCP and RCP components of opposite handedness and phases, each of them travels at different speeds in the medium due to the different refractive indices causing a relative phase shift. This difference in refractive index or MCB is given by

$$\Delta n_{\mathrm{MCB}} = n_+ - n_- = n_L - n_R = i(\mu_0/n_0)\left(\chi_{XYZ}^{(2)eem} + \chi_{YZX}^{(2)eme}\right)H_0 \quad , \tag{14}$$

which results in the Faraday rotation angle (in rad)

$$\alpha = \frac{\pi L}{\lambda}\Delta n_{\mathrm{MCB}} = V(\lambda)B_0 L \quad , \tag{15}$$

with

$$V(\lambda) = \frac{i\pi}{n_0\lambda}\left(\chi_{XYZ}^{(2)eem} + \chi_{YZX}^{(2)eme}\right) = \frac{2i\pi}{n_0\lambda}\chi_{XYZ}^{(2)eem} \quad , \tag{16}$$

using the fact that for an isotropic medium $\chi_{XYZ}^{(2)eem} = \chi_{YZX}^{(2)eme}$. Here, as before, V is the Verdet constant, $B_0 = \mu_0 H_0$ is the longitudinal static magnetic flux density, L is the distance travelled in the medium, and λ is the wavelength of light. Note that the Verdet constant is a real quantity and that the nonlinear magneto-optical susceptibility is purely imaginary in such condition, away from resonance.

As mentioned above, a quasi-static magnetic field can be established, either externally with an electromagnet or by an optically-induced magnetization. In the latter process, called the IFE, an intense circularly polarized light beam at frequency ω passes through an isotropic and *non-absorbing* medium, and interacts with a small volume V containing a finite number of

uncorrelated molecules. Because the beam is intense, it induces to second order in the optical field a static molecular magnetic dipole moment

$$\mathbf{m}^{(2)}(0;\omega,-\omega) = \mu_0^{-1}\boldsymbol{\beta}^{mee}(0;\omega,-\omega):\mathbf{E}(\omega)\mathbf{E}(-\omega) \quad , \tag{17}$$

where $\boldsymbol{\beta}^{mee}(0;\omega,-\omega)$ is the molecular mixed opto-magnetic hyperpolarizability. The process described by Eq. (17) is akin to an optomagnetic rectification, a magnetic analog of optical rectification (Fig. 9).

For the general case of an elliptically polarized light travelling in the medium along the positive *Z*-axis, the associated time-harmonic electric field (in the frequency domain) is given by

$$\mathbf{E}(\omega) = \frac{E_0}{(1+\chi^2)^{1/2}}\left(\widehat{\mathbf{X}} + \chi e^{-i\varphi}\widehat{\mathbf{Y}}\right)e^{-i\omega t} \quad , \tag{18}$$

where χ is an (real) amplitude ratio factor and φ is a relative phase factor. For example, for $\chi = 1$ and $\varphi = \pm\pi/2$, one recovers the circular polarization states given in Eq. (10).

Using Eq. (18), the static molecular magnetic dipole moment collinear with the propagation direction can be written explicitly in terms of components as

$$\begin{aligned} m_z^{(2)}(0;\omega,-\omega) &= \mu_0^{-1}\left[\beta_{zxx}^{mee} + \chi\left(\beta_{zxy}^{mee}e^{i\varphi} + \beta_{zyx}^{mee}e^{-i\varphi}\right) + \chi^2\beta_{zyy}^{mee}\right]\frac{E_0^2}{1+\chi^2} \\ &= \mu_0^{-1}\left[\beta_{zxx}^{mee} + 2i\chi\sin\varphi\,\beta_{zxy}^{mee} + \chi^2\beta_{zyy}^{mee}\right]\frac{E_0^2}{1+\chi^2} \quad , \end{aligned} \tag{19}$$

using the fact that in an isotropic medium, $\beta_{zxy}^{mee} = -\beta_{zyx}^{mee}$ [37]. Here, the lower- and uppercase Cartesian subscripts refer to molecular- and laboratory-fixed frames, respectively.

The macroscopic static magnetization is obtained by performing a statistical averaging of the static molecular magnetic dipole moment over all possible molecular orientations:

$$\begin{aligned} M_0 = M_Z(0) &= N\langle m_z^{(2)}(0;\omega,-\omega)\rangle \\ &= N\mu_0^{-1}\left[\langle\beta_{zxx}^{mee}\rangle + 2i\chi\sin\varphi\,\langle\beta_{zxy}^{mee}\rangle + \chi^2\langle\beta_{zyy}^{mee}\rangle\right]\frac{E_0^2}{1+\chi^2} \quad , \end{aligned} \tag{20}$$

where the angular brackets $\langle\cdots\rangle$ stands for the statistical average and N is the number density of molecules. Because of the isotropic nature of the liquid, $\langle\beta_{zxx}^{mee}\rangle = \langle\beta_{zyy}^{mee}\rangle = 0$, and Eq. (20) reduces to

$$M_0 = \frac{4i\chi\sin\varphi}{(1+\chi^2)n_0 c}\chi_{ZXY}^{(2)mee} I \quad , \tag{21}$$

where $I = (n_0\varepsilon_0 c/2)E_0^2$ is the input irradiance and $\chi_{ZXY}^{(2)mee} = (N/\mu_0\varepsilon_0)\langle\beta_{zxy}^{mee}\rangle$.

Because $1/2\left(\chi_{XYZ}^{(2)eem} + \chi_{YZX}^{(2)eme}\right) = \chi_{XYZ}^{(2)eem} = \chi_{ZXY}^{(2)mee}$, then using the expression of the Verdet constant (Eq. (16)), the static magnetization can be further written as

$$M_0 = \frac{\lambda}{\pi c}\frac{2\chi\sin\varphi}{(1+\chi^2)}VI \quad . \tag{22}$$

For a non-magnetic medium, the longitudinal static magnetic flux density generated by the IFE as function of the input irradiance follows from Eq. (22) and is given by

$$B_0 = \mu_0 M_0 = G(\lambda,\chi,\varphi)VI \quad , \tag{23}$$

with

$$G(\lambda, \chi, \varphi) = \frac{\mu_0 \lambda}{\pi c} H(\chi, \varphi) = \frac{\mu_0 \lambda}{\pi c} \frac{2\chi \sin \varphi}{(1+\chi^2)} \quad , \tag{24}$$

where the characteristic parameters χ and φ are implicit functions of the input polarization state described by the HWP rotation angle ψ (see the section "Determination of the characteristic parameters of the elliptical polarization" of Supplementary Information for more details).

Inserting Eq. (24) into Eq. (15), a similar linear relation between the Faraday rotation angle and the input irradiance can also be established:

$$\alpha = G(\lambda, \chi, \varphi) L V^2 I \quad . \tag{25}$$

Materials. Neat organic liquids including benzene (No. 270709, purity ≥99.9%), chloroform (No. 366927, purity ≥99.8%), and toluene (No. 650579, purity ≥99.9%), chiral liquids (1*S*)-(-)-α-pinene (No. 305715, enantiomeric excess (ee) = 97%) and (1*R*)-(+)-α-pinene (No. 268070, ee ≥ 96.5%), (*R*)-(-)-carvone (No. 124931, purity ≥ 97.5%) and (*S*)-(+)-carvone (No. 435759, purity ≥ 95.5%), as well as europium (III) trifluoromethanesulfonate (No. 425680, purity = 98%) were purchased from Sigma-Aldrich and used as-received. Highly purified water with a resistivity ≥18.0 MΩ·cm from an in-house purification system was used. Liquid samples were contained in amorphous quartz cuvettes purchased from Hellma with either 2- (115-F-10-40, 0.4 mL), 3- (101-015-40, 0.13 mL), 4- (114F-10-40, 1.4 mL), 5- (111-057-40, 0.85 mL), or 10-mm (111-10-40, 3.5 mL) optical path lengths.

Photopolarimetric measurements and data acquisition. Photopolarimetric measurements at 700 nm were carried out using the laser output of an optical parametric amplifier (PG411, Ekspla) pumped by a passively mode-locked neodymium-doped yttrium vanadate (Nd:YVO_4) picosecond laser (PL2210-A-1K-SH, Ekspla). The pulse width (τ) and

the repetition rate (f_{rep}) of laser pulses were ~20–25 ps and 1 kHz, respectively. The intensity of the input beam on the sample was controlled from ~0.1 up to 10 mW by a motorized HWP followed by a Glan-Laser polarizer with its transmission axis fixed vertically. The polarization state of the input beam, which is initially linearly polarized vertically, was varied using a combination of motorized HWP (with a rotation angle ψ) followed by a quarter-wave plate (QWP) with its fast axis fixed vertically. LP input beams were obtained by setting $\psi = 0°$, whereas LCP/LCP beams were obtained with $\psi = \pm 22.5°$. At any other values of ψ, input beams were elliptically polarized. The collimated input beam with a diameter $D \approx 3$ mm was focused down to a beam size of ~10 μm by a near-infrared 5× Mitutoyo objective lens (MY5X-822, Mitutoyo M Plan Apo, Thorlabs; numerical aperture (NA) = 0.14, working distance (WD) = 37.5 mm, effective focal length (EFL) = 40 mm) before passing through the liquid sample contained in a quartz cuvette. The elliptically polarized output beam was analyzed by a motorized rotating polarizer before being detected by a photodetector (PM100D with S121C powerhead, Thorlabs) or an InGaAs photodiode (DET 10N/M Thorlabs) in the case of the photopolarimetric measurements on carvone at 775 nm. Each measurement was averaged over 3 to 10 s. The power and polarization state of the incident beam as well as the settings of the power and polarization scans were controlled by a custom-designed LabView interface.

Photopolarimetric measurements at 1550 nm were performed with a diode-pumped, intra-cavity frequency conversion, Q-switched nanosecond optical parametric oscillator (DC150-1053-OPO, Photonics Industries). The pulse width and the repetition rate of laser pulses were 5 ns and 50 Hz, respectively. The maximal intensity of the input beam on the sample was 7.1 mW. The polarization state of the input beam linearly polarized vertically was controlled in a manner similar to the setup at 700 nm. The collimated input beam with a diameter $D \approx 4$ mm was focused on the sample by a 10× Nikon objective lens (NX10-PF, Nikon Plan Fluor, Thorlabs;

NA = 0.30, WD = 16 mm, EFL = 20 mm). The polarization characteristics of the output beam were analyzed with the same methodology as that of the setup at 700 nm.

All measurements were carried out at ambient temperature (293 K) and pressure.

Data availability

The data that support the findings of this study are available from the corresponding author upon reasonable request.

References

1 Fumagalli, P. & Schoenes, J. *Magneto-optics: An introduction*. (De Gruyter, 2022).

2 Zvezdin, A. K. & Kotov, V. A. *Modern Magneto-Optics and Magneto-Optical Materials*. (Institute of Physics Publishing, 1997).

3 Faraday, M. On the magnetization of light and the illumination of the magnetic lines of force. *Phil. Mag.* **28**, 294-317 (1846).

4 Verdet, É. Recherches sur les propriétés optiques développées dans les corps transparents par l'action du magnétisme. Première partie. *Ann. Chim. Phys.* **41**, 370-412 (1854).

5 Verdet, É. Recherches sur les propriétés optiques développées dans les corps transparents par l'action du magnétisme. Deuxième partie. *Ann. Chim. Phys.* **43**, 37-44 (1855).

6 Verdet, É. Recherches sur les propriétés optiques développées dans les corps transparents par l'action du magnétisme. Troisième partie. *Ann. Chim. Phys.* **52**, 129-163 (1858).

7 Verdet, É. Recherches sur les propriétés optiques développées dans les corps transparents par l'action du magnétisme. Quatrième partie. *Ann. Chim. Phys.* **69**, 415-491 (1863).

8 Verbiest, T., Clays, K. & Rodriguez, V. *Second-Order Nonlinear Optical Characterization Techniques: An Introduction*. (CRC Press, 2009).

9 Shen, Y. R. *The Principles of Nonlinear Optics*. (John Wiley & Sons, 1984).

10 Deeter, M. N., Day, G. W. & Rose, A. H. in *Handbook of Laser Science and Technology, Supplement 2: Optical Materials* (ed M. J. Weber) Ch. 9. Magnetooptic Materials, pp. 367-402 (CRC Press, 1995).

11 Buckingham, A. D. & Stephens, P. J. Magnetic optical activity. *Annu. Rev. Phys. Chem.* **17**, 399-432 (1966).

12 Munin, E. in *Handbook of Laser Science and Technology, Supplement 2: Optical Materials* (ed M. J. Weber) Ch. 9. Magnetooptic Materials, pp. 403-411 (CRC Press, 1995).

13 Balbin Villaverde, A. & Donatti, D. A. Verdet constant of liquids; measurements with a pulsed magnetic field. *J. Chem. Phys.* **71**, 4021-4024 (1979).

14 Ingersoll, L. R. & Liebenberg, D. H. The Faraday effect in gases and vapors. I. *J. Opt. Soc. Am.* **44**, 566-571 (1954).

15 Ingersoll, L. R. & Liebenberg, D. H. Faraday effect in gases and vapors. II. *J. Opt. Soc. Am.* **46**, 538-542 (1956).

16 Vandendriessche, S., Valev, V. K. & Verbiest, T. Faraday rotation and its dispersion in the visible region for saturated organic liquids. *Phys. Chem. Chem. Phys.* **14**, 1860-1864 (2012).

17 Turvey, K. Determination of Verdet constant from combined ac and dc measurements. *Rev. Sci. Instrum.* **64**, 1561-1568 (1993).

18 Brevet-Phillibert, O. & Monin, J. The measurement of the Faraday effect in alternating magnetic fields: A new and simple method. *Meas. Sci. Technol.* **1**, 362-364 (1990).

19 Jain, A., Kumar, J., Zhou, F., Li, L. & Tripathy, S. A simple experiment for determining Verdet constants using alternating current magnetic fields. *Am. J. Phys.* **67**, 714-717 (1999).

20 Valev, V. K., Wouters, J. & Verbiest, T. Precise measurements of Faraday rotation using ac magnetic fields. *Am. J. Phys.* **76**, 626-629 (2008).

21 Suwa, M., Miyamoto, K. & Watarai, H. Faraday rotation dispersion measurements of diamagnetic organic liquids and simultaneous determination of natural optical rotatory dispersion using a pulsed magnetic field. *Anal. Sci.* **29**, 113-119 (2003).

22 Hunte, C. A modulation technique for the measurement of the DC longitudinal Faraday effect. *Eur. J. Phys.* **39**, 025301 (2018).

23 Phelps, G., Abney, J., Broering, M. & Korsch, W. A sensitive Faraday rotation setup using triple modulation. *Rev. Sci. Instrum.* **86**, 073107 (2015).

24 Chang, C.-Y., Wang, L., Shy, J.-T., Lin, C.-E. & Chou, C. Sensitive Faraday rotation measurement with auto-balanced photodetection. *Rev. Sci. Instrum.* **82**, 063112 (2011).

25 Jo, J. Y., Kim, Y., Wangbo, C. K. H. & Kim, K. H. Sensitive measurement of the magneto-optic effect in the near infrared wavelength region with weak alternating magnetic fields. *Opt. Mater. Expr.* **8**, 2636-2642 (2018).

26 van der Ziel, J. P., Pershan, P. S. & Malstrom, L. D. Optically-induced magnetization resulting from the inverse Faraday effect. *Phys. Rev. Lett.* **15**, 190-193 (1965).

27 Pershan, P. S., van der Ziel, J. P. & Malstrom, L. D. Theoretical discussion of the inverse Faraday effect, Raman scattering, and related phenomena. *Phys. Rev.* **143**, 574-583 (1966).

28 Kimel, A. V., Kiriliyuk, A. & Rasing, T. Femtosecond opto-magnetism: ultrafast laser manipulation of magnetic materials. *Laser Photon. Rev.* **1**, 275-287 (2007).

29 Kiriliyuk, A., Kimel, A. V. & Rasing, T. Ultrafast optical manipulation of magnetic order. *Rev. Mod. Phys.* **82**, 2731-2784 (2010).

30 Botek, E., Champagne, B., Verbiest, T., Gangopadhyay, P. & Persoons, A. A joint theoretical-experimental investigation of the Faraday effect in benzene, toluene, and *p*-xylene. *ChemPhysChem* **7**, 1654-1656 (2006).

31 Harrison, N. J. & Jennings, B. R. Laser-induced Kerr constants for pure liquids. *J. Phys. Chem. Ref. Data* **21**, 157-163 (1992).

32 Ingersoll, L. R. Magnetic rotation in various liquids in the short infra-red spectrum. *J. Opt. Soc. Am. Rev. Sci. Instrum.* **6**, 663-681 (1922).

33 Ingersoll, L. R. & Liebenberg, D. H. Faraday effect in gases and vapors. III. *J. Opt. Soc. Am.* **48**, 339-343 (1958).

34 Cataldo, F., Ursini, O. & Angelini, G. Radioracemization and radiation-induced chiral amplification of chiral terpenes measured by optical rotatory dispersion (ORD) spectroscopy. *Radiation Phys. Chem.* **77**, 961-967 (2008).

35 Pershan, P. S. Magneto-optical effects. *J. Appl. Phys.* **38**, 1482-1490 (1967).

36 Wagnière, G. H. *Linear and Nonlinear Properties of Molecules*. 195 p. (VCH Publishers, 1993).

37 Kielich, S. & Zawodny, R. Optical nonlinear phenomena in magnetized crystals and isotropic bodies. *Acta Phys. Polonica A* **43**, 579-602 (1973).

Acknowledgements

This research has been carried out with financial support from the Région Aquitaine (CRA: 2015-1R10205-00004858) and the French State, managed by the French National Research Agency (ANR) in the framework of the project “NLOChiramat” (ANR-21-CE06-0018-03) and of “the Investments for the future” Programme IdEx Bordeaux LAPHIA (ANR-10-IDEX-03-02).

Authors Contributions

D.V. and V.R. designed the project. A.K. and V.R. performed the polarimetric experiments. F.A. conceived and realized the LabView interface. D.V. and V.R. analyzed the data. D.V. and V.R. wrote the manuscript.

Competing interests

The authors declare no competing interests.

Supplementary Files

This is a list of supplementary files associated with this preprint. Click to download.

- OptomagneticeffectsinliquidsSI.pdf